Surface Science 606 (2012) 1790–1797

Contents lists available at SciVerse ScienceDirect

Surface Science

journal homepage: www.elsevier.com/locate/susc

Effect of oxygen gas pressure on orientations of Cu_2O nuclei during the initial oxidation of Cu(100), (110) and (111)

Langli Luo [a], Yihong Kang [b], Judith C. Yang [c], Guangwen Zhou [a,*]

[a] Department of Mechanical Engineering & Multidisciplinary Program in Materials Science and Engineering, State University of New York, Binghamton, NY 13902, United States
[b] Department of Mechanical Engineering and Materials Science, University of Pittsburgh, Pittsburgh, PA 15261, United States
[c] Department of Chemical and Petroleum Engineering, University of Pittsburgh, Pittsburgh, PA 15261, United States

ARTICLE INFO

Article history:
Received 12 April 2012
Accepted 11 July 2012
Available online 23 August 2012

Keywords:
Oxidation
Nucleation
Epitaxy
Copper
In-situ transmission electron microscopy

ABSTRACT

The orientations of oxide nuclei during the oxidation of Cu(100), (110) and (111) surfaces have been examined by in situ transmission electron microscopy. Our results indicate that the epitaxial nucleation of oxide islands on these surfaces cannot be maintained for a whole range of oxygen gas pressure varying from 10^{-5} Torr to 750 Torr. The critical oxygen gas pressure, pO_2, leading to the transition from nucleating epitaxial to non-epitaxial oxide nuclei shows a dependence on the crystallographic orientations of the Cu substrates with $pO_2^{(100)} > pO_2^{(111)} > pO_2^{(110)}$. By fitting the experimentally determined critical oxygen pressures to a kinetic model, we find that such dependence can be attributed to the effect of surface orientations of the Cu substrates on the oxygen surface adsorption and diffusion, which dominate the kinetic processes of oxide nucleation.

1. Introduction

The interaction of clean metal surface and oxygen gas is of significant interests in surface science and also dominates a number of physical and chemical processes including the initial stages of oxidation of metals, gas sensing, and gate oxides [1]. Furthermore, surface oxides play a critical role in heterogeneous catalysis, where the catalytic properties are intimately related to oxidation states of metal atoms and surface morphology of the oxide film formed on the metal surfaces. It has been increasingly apparent that the catalytic active phase for some transitional metals is in fact their oxides rather than the pure metals [2,3].

The oxidation of metals involves hierarchical multiple length scales and proceeds generally from oxygen chemisorption and surface reconstruction to oxide nucleation and growth and then to the formation of a continuous, macroscopically thick oxide layer. Initial stages of metal oxidation refer to the processes before the growth of oxide scales, especially oxygen chemisorption induced surface reconstruction resulting in intermediate sub-oxides or 'pseudo-oxide' [1] and nucleation and growth of stable oxides. Surface reconstructions by the incorporation of gas atoms into metal surface or sub-surface layer have long been investigated by UV-photoelectron spectroscopy (UPS) [4], X-ray photoelectron spectroscopy (XPS) [5], low-energy electron diffraction (LEED) [6,7], and surface X-ray diffraction [8], and have gained tremendous interest after scanning tunneling microscopy (STM) is available for directly imaging surface atoms and structures under ultra-high vacuum (UHV) conditions [9–11]. Cu has been studied as a prototype of transition metals for its surface interaction with oxygen gas [12,13] and a variety of reconstructed structures on the low-index Cu surfaces have been observed, e.g. c(2×2) and $\left(2\sqrt{2}\times\sqrt{2}\right)R45°$ on Cu(100) [14–18]; (2×1) and (6×2) on Cu(110) [19–21]; and '29'- $\left(\sqrt{13}R46.1°\times 7R21.8°\right)$ and '44'-$\left(\sqrt{73}R5.8°\times\sqrt{21}R-10.9°\right)$ structures on Cu(111) [22,23]. A number of mechanisms for the formation of these chemisorption phases on the Cu surfaces are proposed [24–28]. Using these surface science approaches, a wealth of knowledge has been gathered regarding the effect of surface orientations on the oxygen chemisorption induced surface reconstructions. However, little has been reported on the effect of surface orientations on the oxide nucleation and growth such as nucleation kinetics and epitaxial relationship between metal surface and oxide nuclei.

In situ electron microscopy technique is one of the unique approaches for obtaining kinetic data from the initial stages of metal oxidation [29–32]. Real time observation of the nucleation and growth of oxide islands on metal surfaces by in situ environmental transmission electron microscopy (TEM) overcomes the instrumental limitations of traditional experimental techniques. By introducing reactive gas to specimens under elevated temperatures, in situ TEM experiments provide dynamic information from nucleation to growth and coalescence of oxide islands in nanometer scale under the controlled oxidation conditions, which is inaccessible by both surface science and traditional bulk oxidation study methods, but is essential for understanding the atomistic initial-stage oxidation kinetics. On the other hand, most of the studies of initial stages of metal oxidation have been performed under high vacuum conditions while technological applications such as catalytic

* Corresponding author.
E-mail address: gzhou@binghamton.edu (G. Zhou).

0039-6028/$ – see front matter
http://dx.doi.org/10.1016/j.susc.2012.07.042

reactions or oxidation-induced failures in microelectronic devices occur typically under ambient or near atmospheric condition. Therefore, detailed study of the oxidation behavior under practical gas conditions is highly desired and some recent studies revealed that the reaction mechanisms can be indeed significantly different between UHV conditions and ambient gas pressures [3,33–36].

The oxidation of copper and many other metals is observed to proceed via nucleation of oxide islands [37–39]. While it is usually assumed that orientations of oxide islands are controlled by thermodynamics, for which the nucleation of epitaxial oxide islands is favored, we showed recently by in-situ TEM that epitaxial nucleation of oxide islands during the oxidation of Cu(100) surfaces cannot be maintained within the whole range of oxygen pressure [40]. By increasing oxygen gas pressure, there is a transition from nucleating epitaxial oxide islands to randomly oriented oxide islands on Cu(100). In this work, we extend the experiment to the oxidation of Cu(100), (110) and (111) surfaces by comparatively studying the effect of surface orientations on the nucleation orientations of oxide islands under the oxygen gas pressure varying from 5×10^{-5} to 760 Torr. Our study reveals that the transition from nucleating epitaxial Cu_2O nanoislands to non-epitaxial islands occurs for all these three low-index surfaces upon increasing the oxygen gas pressure, thereby demonstrating the broader universality of this phenomenon. However, we also find that the critical oxygen pressure leading to such an orientation transition depends on the surface orientation of the Cu surface. Such surface orientation dependence of the critical oxygen gas pressure is ascribed to a number of kinetic parameters that control the oxide nucleation including oxygen sticking coefficient, activation energy for oxygen desorption and activation energy for oxygen surface diffusion.

2. Experimental

Single crystal Cu(100), (110) and (111) thin films were epitaxially deposited on NaCl(100), (110), and (111) substrates, respectively, in an electron-beam evaporator at 350 °C. The thickness of 700 Å of Cu films was chosen so that the metal films were thin enough to be examined by the TEM but thick enough for the oxidation behavior as close as to that of bulk metal. The Cu thin films were removed from NaCl substrates by floating in deionized water, washed and mounted on a specially designed TEM holder that allows for resistive heating up to ~1000 °C. Our in situ oxidation experiments were carried out in a modified JEOL 200CX TEM. This microscope is equipped with an ultrahigh vacuum (UHV) chamber with a base pressure at $\sim10^{-8}$ Torr. A leak valve attached to the column permits introduction of gasses directly into the TEM sample region with a controlled oxygen gas pressure (pO_2) ranging from 5×10^{-5} Torr to 760 Torr, which can be monitored by a full range vacuum gage. Before the oxidation experiments, any native oxide was removed by annealing in the TEM chamber at 750 °C under vacuum condition [41] or in situ annealing under H_2 gas at pressure $\sim10^{-5}$ Torr and 350 °C, resulting in a clean surface. The sample cleanliness was checked by energy-dispersive X-ray spectroscopy (EDS) analysis and electron diffraction. Oxygen gas of 99.999% purity was then admitted into the column of the microscope through the leak valve to oxidize clean Cu film at 350 °C under a constant pO_2 between 5×10^{-5} Torr and 760 Torr. Real-time TEM observations of the oxidation can be made at pressures $\leq8\times10^{-4}$ Torr. For higher pO_2, the electron gun is isolated from the TEM column during the oxidation, and TEM characterization was made immediately after the oxidation by promptly pumping the TEM column to vacuum. TEM techniques including electron diffraction and bright/dark field imaging were utilized to determine the orientation relationships of oxide islands with the Cu substrates.

3. Results

Incubation period exists before the nucleation of oxide islands under moderate temperature (~350 °C) oxidation. After introducing oxygen gas to the TEM chamber, no oxide islands emerge on the Cu surfaces immediately. After an incubation time, visible embryos of Cu_2O islands can be observed and the number density of oxide islands increases and reaches a saturation density with the continued oxidation. It is observed that the saturation time (the time required for reaching the saturated density of oxide islands) depends on both the oxygen partial pressure and orientation of the Cu surface. In general, for all the three surface orientations, a higher oxygen gas pressure results in a faster oxide nucleation and thus a shorter saturation time. However, for the same oxygen pressure, Cu(100) surface shows the longest saturation time, followed by Cu(111) and then by Cu(110). As shown in Fig. 1, for the oxidation of Cu(100) at 350 °C, the saturation time is ~15 min for $pO_2=5\times10^{-3}$ Torr and it becomes ~5 min for $pO_2=5$ Torr. For the different surface orientations, the saturation time is 15 min for (100), 10 min for (111) and 7 min for (110) surface, respectively, for the oxidation at T = 350 °C and $pO_2=5\times10^{-3}$ Torr.

In situ TEM imaging is used to determine the number density of oxide islands during the oxidation of Cu films. The samples are oxidized for different durations, and it is observed that the island density increases initially and then saturates after a certain period of oxidation time at which individual oxide islands are still clearly visible (and thus the island density can be easily determined by statistically averaging different surface areas). After the saturation density is reached, there is only oxide growth without nucleating new oxide islands, which results in the transition from the growth of discrete islands to the formation of a coalesced oxide film. The measurements indicate that the saturation density of oxide islands depends on both the oxygen gas pressure and surface orientation of the Cu films. Fig. 2 shows the saturation density as a function of the oxygen gas pressure ranging from $pO_2=5\times10^{-4}$ Torr to 500 Torr for the oxidation of Cu films with the different orientations at 350 °C. It can be noted that the island saturation density increases with the oxygen gas pressure for all the Cu surfaces and the saturation density of oxide islands on Cu(100) surface is much lower than Cu(110) and (111) surfaces while Cu(111) surface shows a larger island density than Cu(110) surface for the whole range of the oxygen gas pressure.

The above TEM measurements indicate that the oxide nucleation processes is strongly influenced by oxygen gas pressure and the orientation of the Cu surfaces. The observed dependence of the saturation time for oxide nucleation and saturation density of oxide islands on the oxygen gas pressure (i.e., Figs. 1 and 2) suggests that the oxide nucleation processes is limited by oxygen surface diffusion: the oxide nucleation results from collisions of diffusing oxygen atoms greater than a threshold of the surface density of oxygen atoms. Upon formation, the critical oxide nucleus begins to grow by capturing neighboring oxygen

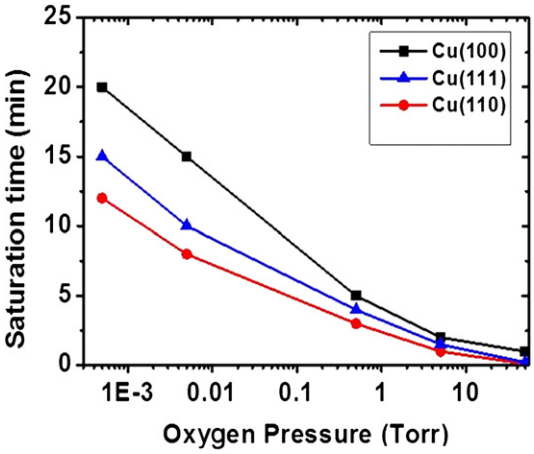

Fig. 1. Dependence of saturation time for reaching the saturated density of oxide islands on the oxygen partial pressure for the oxidation of Cu(100), Cu(110) and Cu(111) at 350 °C.

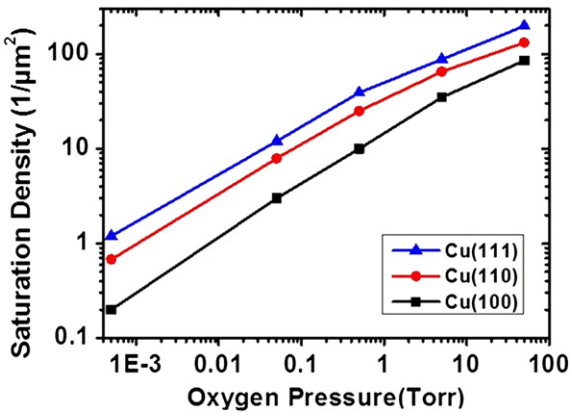

Fig. 2. Dependence of the saturated density of oxide islands on the oxygen gas pressure for the oxidation of Cu(100), Cu(110) and Cu(111) at 350 °C.

atoms, thus leading to a local decrease in the density of oxygen atoms. Due to the locally released supersaturation conditions in oxygen surface density required for oxide island nucleation, the probability of nucleating a second island within this oxygen-depleted region is correspondingly reduced. Therefore, there is an active zone of oxygen captured around individual oxide islands, and the radius of this captured zone is dependent on the surface density and mobility of oxygen atoms. The increase in oxygen gas pressure can significantly increase the oxygen impingement rate for quickly reaching the threshold of oxygen atom density for nucleating oxide islands. Thus, the saturation time decreases while the saturated island density increases with increasing the oxygen gas pressure.

The observed differences in both the saturation time and the density of oxide islands among the three Cu surfaces suggest that the oxygen surface adsorption can be influenced by the Cu surface orientations. The sticking probability for O_2 on Cu surfaces shows a marked crystallographic face dependence. The oxygen surface sticking coefficient is ~0.2 for (110) surface [42], but it is ~0.001 for (100) and (111) surfaces [43], about 2 orders of magnitude lower than Cu(110). Due to the larger oxygen surface sticking coefficient, a faster nucleation rate is thus expected for Cu(110) surface, resulting from a shorter time needed to reach the threshold of surface density of oxygen atoms for nucleating an oxide island.

We then examine the effect of oxygen gas pressure on the nucleation orientations of oxide islands during the oxidation of the Cu films. Fig. 3(a–c) shows dark-field (using Cu_2O (220) diffraction spot) TEM images of a Cu(110) surface oxidized at 350 °C under the different oxygen pressures for 15 min. The saturation density of oxide islands increases with increasing the oxygen partial pressure (note that the dark-field TEM imaging is preferred for better visibility of individual islands due to the large island density). Selected area electron diffraction (SAED) patterns of the oxidized Cu(110) surfaces confirm that the oxide islands formed from the oxidation have a Cu_2O phase. The SAED patterns show a cube-on-cube epitaxial relationship between the oxide islands and the metal substrates for the oxidation at lower oxygen pressures (pO_2<5 Torr), i.e. the orientation relations of (111) Cu_2O//(111)Cu and [011]Cu_2O//[011]Cu are maintained. However, for oxidation under the oxygen pressure $pO_2 \geq 50$ Torr, SAED diffraction ring patterns are obtained, as shown in the lower panel of Fig. 3(c). The ring diffraction patterns imply that the epitaxial nucleation of Cu_2O islands is lost with the metal substrate. The relatively uniform intensity along the diffraction rings suggests that these oxide islands are oriented randomly without preferred orientations.

Similar behavior in the orientation transition from nucleating epitaxial Cu_2O islands to non-epitaxial oxide islands is observed for the oxidation of the other two Cu surfaces, i.e. Cu(100) and Cu(111). Fig. 4 shows bright-field TEM images and the corresponding SAED patterns of a Cu(100) film oxidized at 350 °C with the different oxygen pressures for 15 min. Compared to the Cu(110) surface, the island density dramatically decreases but the average island size increases for the Cu(100) surface. A significant difference from the oxidation of Cu(110) surface is that a higher oxygen gas pressure is needed in order to nucleate non-epitaxial Cu_2O islands on Cu(100) surface. As shown in Fig. 4c, individual oxide islands are visible for the oxidation at $pO_2 = 150$ Torr for 15 min while the diffraction ring pattern indicates that the nucleation of randomly oriented oxide islands has occurred under this pressure. The effect of the Cu crystallographic faces on the orientations of oxide islands is further shown in Fig. 5. Bright-field TEM images and the

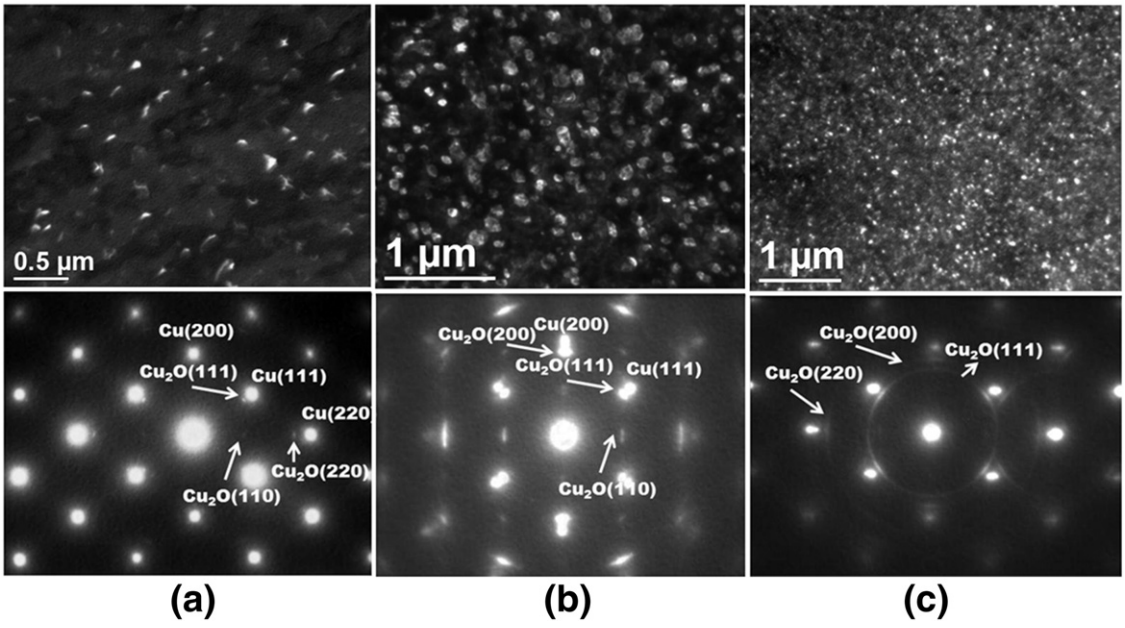

Fig. 3. (Upper panel) TEM images of Cu_2O islands formed on Cu(110) oxidized at 350 °C and different oxygen pressures for 15 min, (a) $pO_2 = 5\times10^{-4}$ Torr, (b) $pO_2 = 0.5$ Torr, and (c) $pO_2 = 50$ Torr; (lower panel) SAED patterns from the corresponding oxidized Cu(110) surfaces. A transition from nucleating epitaxial oxide islands to randomly oriented Cu_2O islands occurs upon increasing the oxygen pressure, as can be seen from the transition of the electron diffraction from the spot pattern to the ring pattern.

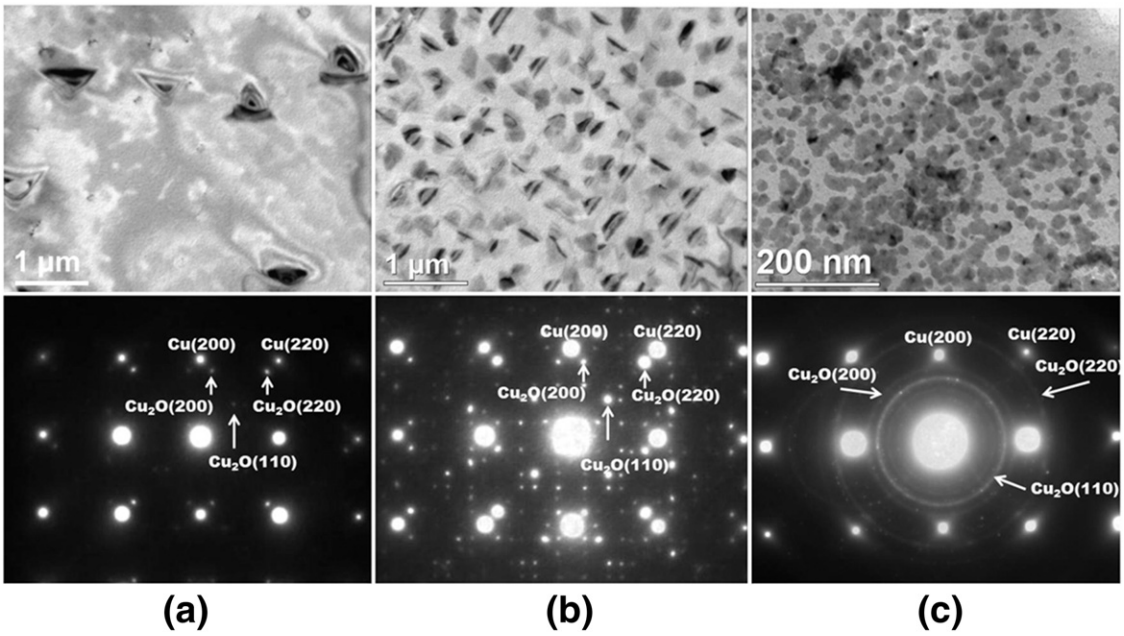

Fig. 4. (Upper panel) TEM images of Cu_2O islands formed on Cu(100) oxidized at 350 °C and different oxygen pressures for 15 min, (a) $pO_2 = 5\times10^{-4}$ Torr, (b) $pO_2 = 0.5$ Torr, and (c) $pO_2 = 150$ Torr; (lower panel) SAED patterns from the corresponding oxidized Cu(100) surfaces, where the additional reflections are due to double diffraction of electron beams by Cu and Cu_2O. A transition from nucleating epitaxial oxide islands to randomly oriented Cu_2O islands occurs upon increasing the oxygen pressure, as can be seen from the transition of the electron diffraction from the spot pattern to the ring pattern.

corresponding SAED patterns of a Cu(111) film oxidized at 350 °C for 15 min with different oxygen pressures show a larger island density and smaller average island size compared with Cu(110). The oxygen pressure required for nucleating randomly oriented oxide islands on Cu(111) surface is ~75 Torr. It is noted that the appearance of additional diffraction spots or rings surrounding the Cu reflections in the electron diffraction patterns shown in Figs. 4 and 5 is caused by the double diffraction of Cu_2O islands and the Cu substrates.

The above TEM observations indicate that increasing the oxygen gas pressure results in the transition from forming epitaxial oxide islands to non-epitaxial islands for all the three Cu surfaces. Nevertheless, it is crucial to elucidate whether the observed transition in the island orientations is related to the initial stage of oxide nucleation or the subsequent stage of oxide growth and coalescence that may cause deviation from the initial orientations of oxide islands. We therefore examined the effect of growth and coalescence of oxide islands on the orientations of the resulting oxide film by monitoring the orientation evolution as a function of oxidation time. Fig. 6 shows bright-field TEM images and the corresponding SAED patterns obtained from the oxidation of Cu(110) surfaces at $pO_2 = 50$ Torr

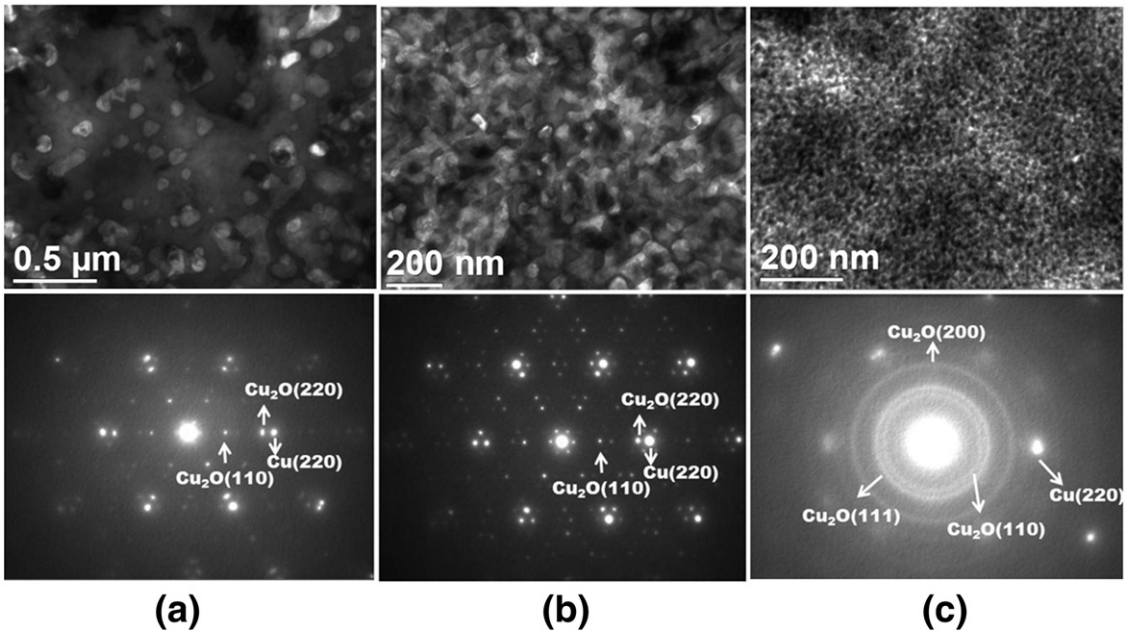

Fig. 5. (Upper panel) TEM images of Cu_2O islands formed on Cu(111) oxidized at 350 °C and different oxygen pressures for 15 min, (a) $pO_2 = 5\times10^{-4}$ Torr, (b) $pO_2 = 0.5$ Torr, and (c) $pO_2 = 75$ Torr; (lower panel) SAED patterns from the corresponding oxidized Cu(111) surfaces, where the additional reflections are due to double diffraction of electron beams by Cu and Cu_2O. A transition from nucleating epitaxial oxide islands to randomly oriented Cu_2O islands occurs upon increasing the oxygen pressure, as can be seen from the transition of the electron diffraction from the spot pattern to the ring pattern.

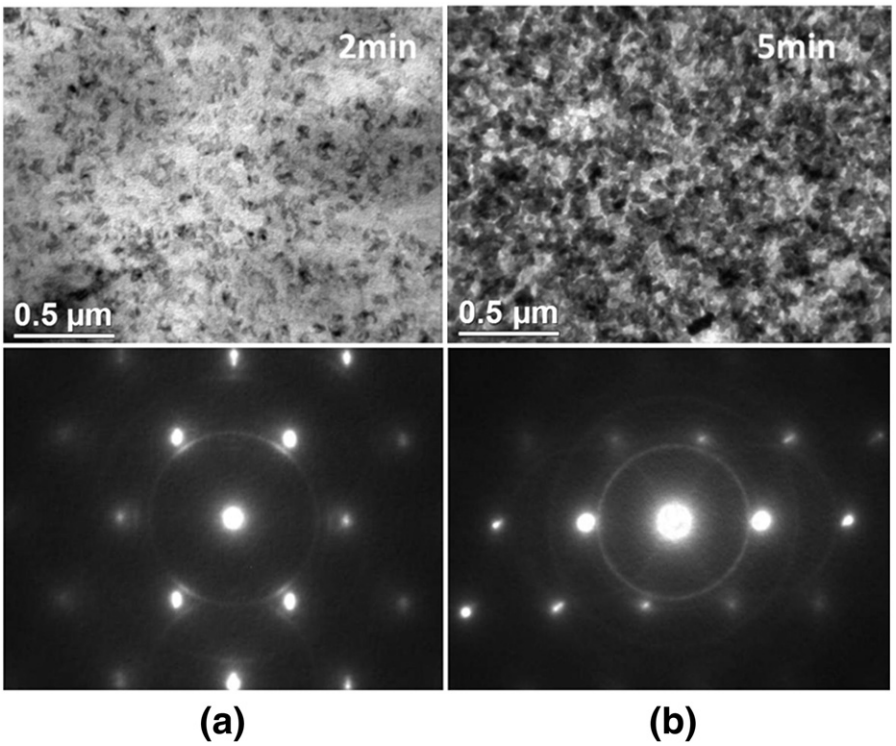

Fig. 6. Upper panel: Bright-field TEM images of Cu_2O islands formed on Cu(110) oxidized at 350 °C and $pO_2 = 50$ Torr for (a) 2 min, (b) 5 min. Lower panel: SAED patterns from the corresponding oxidized Cu(110) surfaces. The observed ring patterns reveal that the cube-on-cube epitaxial orientation is lost in the initial stage of oxide nucleation under this oxygen pressure.

and 350 °C for 2 and 5 min, respectively. As shown in Fig. 6a, after the oxidation of 2 min, visible oxide nuclei appear on the surface and electron diffraction from the oxidized surface already exhibits a diffraction ring pattern, suggesting the formation of randomly oriented oxide islands in the initial-stage oxidation of oxide nucleation. As the oxidation proceeds to 5 min, oxide nuclei grow, coalesce, and develop into a continuous film, which results in stronger intensity in the diffraction ring pattern. The observation suggests that oxide islands nucleate with random orientations with the metal substrate if the oxygen pressure is higher than the critical oxygen pressure required for the orientation transition, where the term "critical nucleation pressure" is defined experimentally as the oxygen pressure at which the diffraction ring pattern is firstly observed.

We then check if the epitaxial to non-epitaxial transition occurs during the oxide growth when the oxygen gas pressure is lower than the critical pressure for the orientation transition. Fig. 7 shows bright-field TEM images and the corresponding SAED patterns obtained from the oxidation of Cu(111) surfaces at 350 °C for 30 min with the oxygen gas pressures of $pO_2 = 5$ Torr and 50 Torr, respectively (note that the oxygen pressure required for forming non-epitaxial Cu_2O islands on Cu(111) surface is ~75 Torr). As shown in Fig. 7a, oxide islands are still visible for $pO_2 = 5$ Torr, and the epitaxial relationship of the oxide islands with the Cu(111) substrates are still maintained despite the longer oxidation time compared to Fig. 5, where the Cu(111) sample was oxidized for only 15 min. For the oxidation at $pO_2 = 50$ Torr, oxide islands have already coalesced to form a continuous oxide film, as shown in the Fig. 7b and the SAED pattern shows that the oxide film is still epitaxial with the Cu(111) substrate. This observation suggests that oxide islands undergo no significant change in crystallographic orientations during the oxide island growth and coalescence. Similar experiments were performed on Cu(100) and (110) samples and it is found that the epitaxial relation of oxide islands (and the continuous oxide films after coalescence) with the Cu substrates is maintained during continued oxidation if the oxygen gas pressure is below the critical oxygen pressure for nucleating non-epitaxial oxide islands. These observations indicate that the orientations of oxide islands are largely determined in the stages of oxide nucleation rather than from the subsequent stages of oxide growth.

While the density, lateral size, and orientations of oxide islands vary significantly with increasing the oxygen pressure, the thickness (height) of the oxide islands formed under the different oxygen pressures is similar for similar oxidation duration, as revealed by ex situ atomic force microscopy of the Cu surfaces oxidized under the different oxygen pressure. This is because the thickening of oxide islands requires bulk diffusion of reactants, which is much slower than surface diffusion. Thus, the oxide growth is dominated by lateral growth prior to the coalescence of oxide islands that switches off routes for surface diffusion.

4. Discussion

The in situ TEM results described above demonstrate that the nucleation of epitaxial oxide islands cannot be maintained for the whole range of the oxygen gas pressure. The critical oxygen gas pressure pO_2 leading to nucleating non-epitaxial oxide islands depends on the crystallographic orientations of the Cu substrates with $pO_2^{(100)} > pO_2^{(111)} > pO_2^{(110)}$. To understand such dependence, we have to elucidate the effect of surface orientations on the oxide nucleation process. Considering the nucleation of a three-dimensional oxide island on a plane metal surface, the oxide nucleation rate, which is defined as the number of stable nuclei created per area-time, J, can be expressed as [40]

$$\frac{J}{B^*} = J_0 a_0 s \times \exp\left(-\frac{16\pi\Omega^2(2+n)(1-n)^2}{3(kT)^3\left[\ln\left(\frac{pO_2}{pO_2^e}\right)\right]^2}\sigma_{NO}^3\right), \quad (1)$$

with $J_0 = \left[\frac{4(1+n)}{(2+n)(1-n)}\right]^{1/2} \times \left(\frac{pO_2}{pO_2^e}\right) \times \ln\left(\frac{pO_2}{pO_2^e}\right) \exp\left(\frac{E_{des}-E_{sd}}{kT}\right)$ and $B^* = \frac{N_0 pO_2^e}{4\sqrt{2\pi m\sigma_{NO}}}$, where J_0 can be called the collisional pre-factor, E_{des} is the activation energy for desorption, E_{sd} is the activation energy

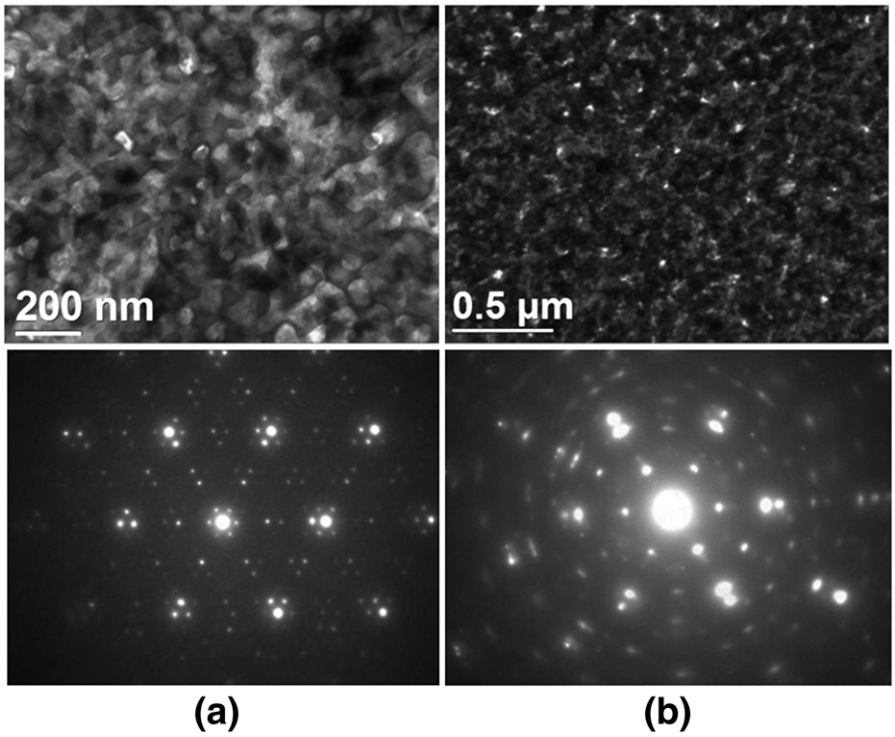

Fig. 7. Upper panel: Bright-field TEM images of Cu_2O islands formed on Cu(111) surface oxidized at 350 °C and the different oxygen pressures for 30 min: (a) $pO_2 = 5$ Torr, (b) $pO_2 = 50$ Torr (note the oxygen pressure required for nucleating non-epitaxial oxide islands for Cu(111) surface is 75 Torr). Lower panel: SAED patterns from the corresponding oxidized Cu(111) surfaces. The observations reveal that the cube-on-cube epitaxial orientation is still maintained during the growth and coalescence processes of the oxide islands.

for surface diffusion, Ω is the volume of oxygen atoms in the oxide phase, m is the molecular mass of oxygen, k is the Boltzmann's constant, T is the oxidation temperature, pO_2 is the oxygen gas pressure, and pO_2^e is the equilibrium oxygen pressure as given by the Ellingham diagram for most metal oxides [44]. n depends on the interaction and structural match between the oxide nucleus and the metal substrate, and is related to the interfacial tension between the oxide and metal substrate by,

$$n = (\sigma_{SO} - \sigma_{NS})/\sigma_{NO}, \tag{2}$$

where σ_{NO}, σ_{NS} and σ_{SO} are the interfacial free energies between the oxide nucleus and oxygen gas, the oxide nucleus and metal substrate, and the metal substrate and oxygen gas, respectively. For a given system, the strong interaction and ideal structural match (i.e., epitaxial nucleation) leads to $n \to 1$; on the other hand, the weak interaction and poor structural match (i.e., nonepitaxial nucleation) leads to $n \to -1$ [45].

In this model, the distance of diffusion jump a_0, the oxygen sticking coefficient s, the activation energy E_{sd} for O surface diffusion and the oxygen desorption energy E_{des} are all face sensitive parameters. Cu(111) has the most close-packed surface atoms, resulting in a smaller jump distance of oxygen atoms than those of the more open (100) and (111) surfaces, i.e. $a_0 = 1.8$ Å for (100) surface, $a_0 = 1.8$ Å or 2.55 Å for (110) surface and $a_0 = 0.73$ Å for (111) surface by assuming that oxygen atoms sit at the most stable FCC hollow sites and diffuse to the nearest neighbor hollow sites for clean surfaces. E_{des} can be approximately equated to the enthalpy of oxygen adsorption since the activation energy for adsorption is often very small [46]. The enthalpy of O adsorption ΔE_{ad} as well as O surface diffusion barrier E_{sd} cannot be obtained by current experimental techniques but have been reported on Cu surfaces through simulation methods such as first principal calculation, i.e. ΔE_{ad} and E_{sd} are ~1.33 eV and ~0.4 eV for Cu(100) [47], ~4.18 eV and ~0.3 eV for Cu(110) [48], and ~2.8 eV and ~0.25 eV [49] for Cu(111) surface, respectively. Note that these energies correspond to the surfaces with the maximum oxygen surface coverage reached by the oxygen chemisorption induced surface restructuring before the onset of oxygen subsurface adsorption due to the large oxygen exposure under the high oxygen gas pressure. By substituting these values of a_0, s, E_{des} and E_{sd} for the three Cu surfaces into Eq. (1), one can obtain the nucleation rate J as a function of the interaction parameter n for different pO_2. As an example, Fig. 8a shows the oxidation of Cu(110) at 350 °C. As seen in the plots, the oxidation of the Cu(110) is dominated by epitaxial nucleation of oxide islands (e.g. $n = 1$) for the low oxygen pressure. With the increase in oxygen gas pressure, the non-epitaxial nucleation (e.g. $n = -1$) of oxide islands is promoted and the difference in nucleation rates between epitaxial and non-epitaxial nucleation is dramatically reduced. Therefore, both epitaxial and non-epitaxial oxide islands are nucleated simultaneously on the surface under the high oxygen pressure. This can be evidenced from the electron diffraction patterns as shown in Fig. 3(b), the diffraction spots start to widen, indicating the emergence of non-epitaxial oxide nuclei under the oxygen pressure $pO_2 = 5$ Torr. Therefore, the range of oxygen pressure between 5 and 50 Torr corresponds to the transition regime of nucleating partly epitaxial and non-epitaxial oxide islands. This observation is in accordance with the trend of the plot $pO_2 = 0.5$ Torr in Fig. 8a that shows a much larger nucleation rate when n approaches 0 or even −1 where non-epitaxial nucleation is promoted.

The effect of the Cu surface orientation on the orientations of oxide islands is illustrated in Fig. 8b. The nucleation rate J/B is plotted via n for the oxidation of Cu(100), (110) and (111) at 350 °C under the same oxygen pressure ($pO2 = 100$ Torr). As can be seen from the plots, the oxidation of Cu(100) surface is dominated by epitaxial nucleation of oxide islands while non-epitaxial nucleation of oxides is highly promoted for Cu(110) and (111) surfaces for the same oxygen gas pressure, i.e., both epitaxial and non-epitaxial oxide islands are nucleated simultaneously on the Cu(110) and (111) surfaces. It can be seen that the Cu(100) surface requires higher critical oxygen pressure for nucleating non-epitaxial oxide islands than Cu(110) and (111). The quantitative

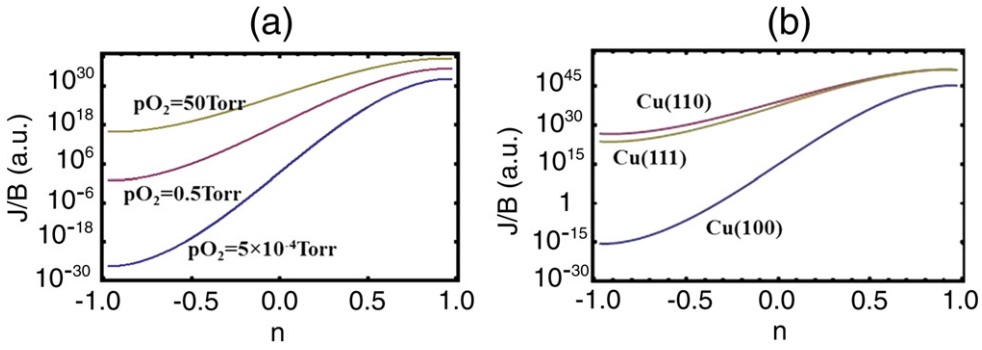

Fig. 8. (a). Plots of the relative steady-state nucleation rate ***J/B*** vs. the interaction parameter **n** at the different oxygen pressure pO_2 for oxidation of Cu(110) at 350 °C; (b). Plots of the relative steady-state nucleation rate ***J/B*** vs the interaction parameter **n** for the oxidation of Cu(100), Cu(110) and Cu(111) at $pO_2 = 100$ Torr and T = 350 °C.

comparison between the nucleation rates of experimental data and the model by Eq. (1) cannot be made due to the lack of the accurate values of surface and interface energies and the surface diffusion rates as a function of oxygen pressure. But the experimental data of the oxygen gas pressures are utilized in the model to predict the effect of oxygen gas pressure and surface orientation on the nucleation orientations of oxide islands during the oxidation. The outcome of the model as shown in Fig. 8 provides reasonable match with the ranges of the oxygen pressure at which the orientation transitions of oxide islands from epitaxial to nonepitaixal nucleation are experimentally observed for the three surface orientations of Cu, where the oxygen pressure leading to nucleation of randomly oriented oxide islands are ~150 Torr for Cu(100), ~75 Torr for Cu(111) and ~50 Torr for Cu(110), respectively. In addition, the model calculations show that the nucleation rate of oxide islands on Cu(110) is slightly faster than that for Cu(111) (Fig. 8b). This trend is in line with the experimental observations. As shown in Figs. 1 and 2, while Cu(111) has a larger density of oxide islands than Cu(110), the oxidation time leading to the island saturation is also longer for Cu(111), which results in a slower overall oxide nucleation rate for the oxidation of Cu(111).

It is clear from the above discussion that epitaxial nucleation of oxide islands can be lost with increasing the oxygen partial pressure and the oxidation of the Cu(100), (110), and (111) surfaces results in the different critical oxygen pressures leading to this orientation transition of oxide islands. Such an effect of the surface orientation on the epitaxial relation of oxide nuclei can be understood as follows. The nucleation rate of oxide nuclei is determined by two competing factors, i.e., nucleation barrier and the effective atom collision rate. At the low oxygen pressure, the nucleation barrier is high, i.e., the nucleation rate is dominated by the exponential term in Eq. (1). The top priority to accelerate the nucleation kinetics is to lower the nucleation barrier. Therefore, heterogeneous nucleation with the strong interaction and good structural match ($n \rightarrow 1$) between an oxide island and the metal substrate will be kinetically favored. Conversely, at high oxygen pressures, the nucleation barrier is reduced and the issue of effective collisions of oxygen atoms, described by the collisional pre-factor, J_0, becomes more important. The nucleation of oxide islands with weak interaction and poor structural match ($n \rightarrow 0$, and -1) with the substrate is enhanced. Therefore, the nucleation barrier term favors epitaxial nucleation while the effective collision term J_0 prefers the nucleation of randomly oriented oxide islands.

The orientations of the substrate surfaces can affect the critical oxygen pressure for the transition to nucleating non-epitaxial oxide nuclei via modification of the effective collision rate term, through its effect on the oxygen sticking coefficient and the oxygen surface diffusion. The oxygen surface sticking coefficients for Cu(100) and (111) are two orders of magnitude smaller than Cu(110) [42,43], which is consistent with the trend by DFT calculations of the oxygen adsorption energies, i.e., 1.33 eV for Cu(100) [47], 4.18 eV for Cu(110) [48] and 2.8 eV for Cu(111) [49]. Therefore, a larger oxygen partial pressure is expected for Cu(100) and (111) in order to reach the critical coverage of oxygen atoms leading to oxide nucleation. We then compare the surface mobility of oxygen on Cu(100) and (111). The surface diffusion barriers for oxygen on Cu(100) and (111) are ~0.4 eV and 0.25 eV, respectively [47,49]. Therefore, Cu(111) surface shows more efficient collision of oxygen atoms for oxide nucleation and a smaller oxygen gas pressure is needed to nucleate non-epitaxial oxide islands. Thus, the observed trend of the difference in magnitude of the critical oxygen pressures, $pO_2^{(100)} > pO_2^{(111)} > pO_2^{(110)}$, for nucleating non-epitaxial oxide islands on the three low-index Cu surfaces can be reasonably ascribed to the interplay among the oxygen surface sticking probability, oxygen adsorption, and effective atom collision in dominating the kinetic processes of oxide nucleation.

5. Conclusion

In conclusion, an orientation transition from nucleating epitaxial to non-epitaxial Cu_2O islands is observed by increasing the oxygen pressure during the initial stages of oxidation of Cu(100), (110) and (111) surfaces. The effect of the surface orientations on the critical oxygen pressure required for such an orientation transition of oxide nuclei is monitored by in situ environmental TEM. It is found that the critical oxygen pressures nucleating non-epitaxial oxide nuclei vary with the surface orientation, e.g. 150 Torr for Cu(100), 50 Torr for Cu(110) and 75 Torr for Cu(111). Such a crystal face dependence of the critical oxygen gas pressure is attributed to the effect of the Cu surface orientation on the oxygen sticking adsorption and oxygen surface mobility that dominate the effective collision rates of oxygen atoms during the oxide nucleation.

Acknowledgment

Research was supported by the U.S. Department of Energy, Office of Basic Energy Sciences, Division of Materials Sciences and Engineering under Award No. DE-FG02-09ER46600.

References

[1] K.R. Lawless, Rep. Prog. Phys. 37 (1974) 231.
[2] H. Over, Y.D. Kim, A.P. Seitsonen, S. Wendt, E. Lundgren, M. Schmid, P. Varga, A. Morgante, G. Ertl, Science 287 (2000) 1474.
[3] R. Westerstrom, J. Gustafson, A. Resta, A. Mikkelsen, J.N. Andersen, E. Lundgren, N. Seriani, F. Mittendorfer, M. Schmid, J. Klikovits, P. Varga, M.D. Ackermann, J.W.M. Frenken, N. Kasper, A. Stierle, Phys. Rev. B 76 (2007) 155410.
[4] H.P. Bonzel, C.R. Helms, S. Kelemen, Phys. Rev. Lett. 35 (1975) 1237.
[5] A.F. Carley, P.R. Davies, R.V. Jones, K.R. Harikumar, M.W. Roberts, Surf. Sci. 490 (2001) L585.
[6] D. Heskett, A. Baddorf, E.W. Plummer, Surf. Sci. 195 (1988) 94.
[7] H. Niehus, Surf. Sci. 130 (1983) 41.
[8] I.K. Robinson, D.J. Tweet, Rep. Prog. Phys. 55 (1992) 599.
[9] M. Bode, R. Pascal, R. Wiesendanger, Surf. Sci. 344 (1995) 185.
[10] H. Tanaka, J. Yoshinobu, M. Kawai, Surf. Sci. 327 (1995) L505.

[11] A.S. Dakkouri, Solid State Ionics 94 (1997) 99.
[12] A. Spitzer, H. Lüth, Surf. Sci. 118 (1982) 121.
[13] A. Spitzer, H. Lüth, Surf. Sci. 118 (1982) 136.
[14] F. Jensen, F. Besenbacher, E. Laegsgaard, I. Stensgaard, Phys. Rev. B 42 (1990) 9206.
[15] T. Kangas, K. Laasonen, Surf. Sci. 606 (2012) 192.
[16] K. Lahtonen, M. Hirsimäki, M. Lampimaki, M. Valden, J. Chem. Phys. 129 (2008) 124703.
[17] M. Ahonen, M. Hirsimäki, A. Puisto, S. Auvinen, M. Valden, M. Alatalo, Chem. Phys. Lett. 456 (2008) 211.
[18] M. Lee, A.J.H. McGaughey, Surf. Sci. 604 (2010) 1425.
[19] D. Coulman, J. Wintterlin, J.V. Barth, G. Ertl, R.J. Behm, Surf. Sci. 240 (1990) 151.
[20] L. Sun, M. Hohage, R. Denk, P. Zeppenfeld, Phys. Rev. B 76 (2007).
[21] X. Duan, O. Warschkow, A. Soon, B. Delley, C. Stampfl, Phys. Rev. B 81 (2010) 075430.
[22] F. Jensen, F. Besenbacher, E. Lægsgaard, I. Stensgaard, Surf. Sci. Lett. 259 (1991) L774.
[23] F. Jensen, F. Besenbacher, I. Stensgaard, Surf. Sci. 269–270 (1992) 400.
[24] F. Besenbacher, J.K. Norskov, Prog. Surf. Sci. 44 (1993) 5.
[25] R. Feidenhans, F. Grey, M. Nielsen, F. Besenbacher, F. Jensen, E. Laegsgaard, I. Stensgaard, K.W. Jacobsen, J.K. Norskov, R.L. Johnson, Phys. Rev. Lett. 65 (1990) 2027.
[26] K. Kern, H. Niehaus, A. Schatz, P. Zeppendfeld, J. Goerge, G. Comsa, Phys. Rev. Lett. 67 (1991) 855.
[27] N. Hartmann, R.J. Madix, Surf. Sci. 488 (2001) 107.
[28] F. Jensen, F. Besenbacher, E. Lasgaard, Phys. Rev. B 41 (1990) 10233.
[29] G. Zhou, J.C. Yang, Surf. Sci. 531 (2003) 359.
[30] G. Zhou, J.C. Yang, Surf. Sci. 559 (2004) 100.
[31] G. Zhou, J.C. Yang, J. Mater. Res. 20 (2005) 1684.
[32] G. Zhou, X. Chen, D. Gallagher, J.C. Yang, Appl. Phys. Lett. 93 (2008) 123104.
[33] E. Lundgren, J. Gustafson, A. Mikkelsen, J.N. Andersen, A. Stierle, H. Dosch, M. Todorova, J. Rogal, K. Reuter, M. Scheffler, Phys. Rev. Lett. 92 (2004) 046101.
[34] S. Ferrer, M.D. Ackermann, E. Lundgren, MRS Bull. 32 (2007) 1010.
[35] K. Lahtonen, M. Hirsimaki, M. Lampimaki, M. Valden, J. Chem. Phys. 129 (2008) 124703.
[36] J.A. Eastman, P.H. Fuoss, L.E. Rehn, P.M. Baldo, G.W. Zhou, D.D. Fong, L.J. Thompson, Appl. Phys. Lett. 87 (2005) 051914.
[37] K. Heinemann, D.B. Rao, D.L. Douglass, Oxid. Met. 9 (1975) 379.
[38] J.C. Yang, M. Yeadon, B. Kolasa, J.M. Gibson, Appl. Phys. Lett. 70 (1997) 3522.
[39] G. Zhou, J.C. Yang, Appl. Surf. Sci. 210 (2003) 165.
[40] L. Luo, Y. Kang, Z. Liu, J.C. Yang, G. Zhou, Phys. Rev. B 83 (2011) 155418.
[41] G.W. Zhou, J.C. Yang, Phys. Rev. Lett. 93 (2004) 226101.
[42] A. Nesbitt, A.K. Lewin, A. Hodgson, J. Phys. Condens. Matter 3 (1991) S71.
[43] F.H.P.M. Habraken, E.P. Kieffer, G.A. Bootsma, Surf. Sci. 83 (1979) 45.
[44] D.R. Gaskell, Introduction to Metallurgical Thermodynamics, Scripta, Washington, D.C., 1973.
[45] X.Y. Liu, J. Chem. Phys. 111 (1999) 1628.
[46] K.K. Kolasinski, Surface Science: Foundations of Catalysis and Nanoscience, Wiley, 2012.
[47] T. Kangas, K. Lassonen, A. Puisto, H. Pitkanen, M. Alatalo, Surf. Sci. 584 (2005) 62.
[48] S.Y. Liem, G. Kresse, J.H.R. Clarke, Surf. Sci. 415 (1998) 194.
[49] A. Soon, M. Todorova, B. Delley, C. Stampfl, Phys. Rev. B 73 (2006) 165424.